Published in final edited form as:
Langmuir. 2007 May 22; 23(11): 6281–6288. doi:10.1021/la063719e.

Specific Adsorption of Histidine-Tagged Proteins on Silica Surfaces Modified with Ni^{2+}:NTA-Derivatized Poly(Ethylene Glycol)

Eunah Kang[1], **Jin-won Park**[2], **Scott McClellan**[2], **Jong-Mok Kim**[4], **David Holland**[4], **Gil U. Lee**[2], **Elias Franses**[2], **Kinam Park**[1,3], and **David H. Thompson**[4]

1 *School of Biomedical Engineering, Purdue University, West Lafayette, IN 47907*

2 *School of Chemical Engineering, Purdue University, West Lafayette, IN 47907*

3 *Department of Pharmaceutics, Purdue University, West Lafayette, IN 47907*

4 *Department of Chemistry, Purdue University, West Lafayette, IN 47907*

Abstract

Silica surfaces modified with nitrilotriacetic acid (NTA)-polyethylene glycol (PEG) derivatives were used for immobilizing hexahistidine-tagged green fluorescent oprotein (his_6-GFP), biotin/streptavidin-AlexaFluor555 (his_6-biotin/SA-AF) and gramicidin A-containing vesicles (his_6-gA). Three types of surface-reactive PEG derivatives—NTA-PEG3400-$Si(OMe)_3$, NTA-PEG3400-vinylsulfone, and mPEG5000-$Si(OMe)_3$ (control)—were grafted onto silica and tested for their ability to capture his_6-tag species via his_6:Ni^{2+}:NTA chelation.

The composition and thicknesses of the PEG-modified surfaces were characterized using x-ray photoelectron spectroscopy, contact angle, and ellipsometry. Protein capture efficiencies of the NTA-PEG-grafted surfaces were evaluated by measuring fluorescence intensities of these surfaces after exposure to his_6-tag species. XPS and ellipsometry data indicate that surface adsorption occurs via specific interactions between the his_6-tag and the Ni^{2+}:NTA-PEG-grafted surface. Protein immobilization was most effective for NTA-PEG3400-$Si(OMe)_3$-modified surfaces, with maximal areal densities achieved at 45 pmol/cm^2 for his_6-GFP and 95 fmol/cm^2 for his_6-biotin/SA-AF. Lipid vesicles containing his_6-gA in a 1:375 gA:lipid ratio could also be immobilized on Ni^{2+}:NTA-PEG3400-$Si(OMe)_3$-modified surfaces at 0.5 mM total lipid. Our results suggest that NTA-PEG-$Si(OMe)_3$ conjugates may be useful tools for immobilizing his_6-tag proteins on solid surfaces to produce protein-functionalized surfaces.

Introduction

Supported lipid membranes are widely studied for biophysical characterization of lipid membranes and are now emerging as an important platform for integral membrane protein biosensors.[1–5] This ambitious goal will require sensors that have been designed with (1) stable and fluid membranes; (2) polymer grafted surfaces to prevent membrane protein inactivation via adsorption onto the solid support; and (3) ligands that enable specific binding and orientation of the membrane protein since their transport and/or catalytic functions are vectorial in nature. Development of methods that improve the stability and controlled orientation of proteins will have a direct impact on the performance of membrane protein-based devices.

Correspondence to: Professor David H. Thompson, Department of Chemistry, Purdue University, 560 Oval Drive, West Lafayette, IN, 47907, Tel: 765-494-0386, E-mail: davethom@purdue.edu.

The first challenge of stabilizing supported lipid membranes is required to block the opportunities for bilayer membrane delamination[a] in areas of the surface where defects can promote membrane instability. The second goal is being addressed by covalently anchoring the membrane to the surface using hydrophilic tethers to increase adhesion and stability of supported lipid membranes.[2–8] An alternative strategy has been the use of polysaccharide-, polyacrylamide-, and polyethylene glycol(PEG)-based lipopolymers to provide a hydrophilic cushion between the supported membrane and the solid support.[9–18] Studies with PEG-grafted surfaces have shown that nanometer-scale aqueous reservoirs could be formed beneath the supported membrane, allowing for enhanced stability of the lipid membrane.[13,14,18] This strategy, however, can decrease lipid lateral mobility due to membrane-solid substrate contact and promote protein adsorption and inactivation due to surface-mediated unfolding.[19,20]

These advances, however, have not fully addressed the third requirement of introducing membrane protein components into the supported membrane in an oriented fashion. Asymmetric orientation of the his-tag molecules has been achieved through metal-mediated complexation of nitrilotriacetic acid (NTA) conjugates and hexahistidine-tagged (his_6-) proteins on silica [21–24] and gold [25–30] surfaces. The alkyl-NTA and oligoethylene glycol-NTA derivatives reported thus far, however, may not be large enough to retain the activity of ABC transporters[b] and other membrane proteins with extensive water-soluble domains.[18] We sought to develop materials that would entrap aqueous reservoirs of controlled dimensions between the membrane and the solid support while providing control over protein orientation, aspects that will be essential for successful development of membrane protein-based biosensors.

This study examines the effectiveness of different PEG-NTA conjugation strategies in specifically binding and orienting his_6-tagged proteins. His_6-tag green fluorescence protein (his_6-GFP), his_6-tag biotin/streptavidin-AlexaFluor555 (his_6-biotin/SA-AF), and lipid vesicles containing his_6-tag gramicidin A (his_6-gA) were used as probes to monitor the adsorption of his_6-tag proteins on PEG-modified surfaces in the presence and absence of NTA derivatives. Protein adsorption on Ni^{2+}:NTA-PEG-modified surfaces in the absence of his_6-tags was also examined as a control. Our experiments show that specific and reversible binding to PEG-modified silica surfaces occurred only when the PEG molecule contained a Ni^{2+}-activated NTA ligand and the protein possessed a hexahistidine interaction with the Ni^{2+}:NTA-PEG-grafted surface.

Experimental Methods

Materials

N-Hydroxysuccinimidyl-PEG3400-vinylsulfone (NHS-PEG3400-VS) and methoxy-PEG5000-silane (mPEG5000-$Si(OMe)_3$) were purchased from Nektar Therapeutics (Huntsville, AL). *N*-Carbobenzyloxy-*L*-lysine was purchased from Aldrich (St. Louis, MO). Gramicidin A was purchased from Fluka (St. Louis, MO). His_6-gA was prepared by custom peptide synthesis and supplied in *C*-terminal hexahistidine form by Abgent, Inc. (San Diego, CA). Egg yolk phosphatidylcholine (EPC) and *L*-α-dioleoylphosphatidylethanolamine (DOPE) were obtained from Sigma (St. Louis, MO). AlexaFluor 555-labeled streptavidin (SA-AF) and *L*-α-dipalmitoylphosphatidylethanolamine-*N*-NBD (NBD-DPPE) were purchased from Molecular Probes (Eugene, OR). His_6-biotin was purchased from Biopeptide Co. (San Diego, CA) and (3-mercaptopropyl)trimethoxysilane (MPTS) was from Gelest Inc.

[a]It is anticipated that delamination can occur either between the membrane and the underlying support or between the apposed monolayers of the bilayer membrane when they are exposed to shear stresses or osmotic stresses.

[b]For example, the intracellular loop and nucleotide binding domains of Sav1866, an ABC transporter from *S. aureus*, is estimated to extend nearly 50 Å beyond the membrane surface.[31]

(Morrisville, PA). All other solvents and reagents were purchased from Aldrich. ^{1}H NMR spectra were recorded using a Bruker ARX300 spectrometer operating at 300MHz. Chemical shifts are reported in ppm relative to the residual solvent peak as internal standard.

Synthesis of NTA intermediate

Lysine nitrilotriacetic acid (NTA) was synthesized as shown in Scheme 1 using a method that has been previously reported.[32,33]

Synthesis of NTA-PEG3400-Si(OMe)$_3$

NTA-PEG3400-VS—NHS-PEG3400-VS (0.85 g, 0.25 mol) and NTA (0.33 g, 1.25 mmol) were dissolved in 8.5 ml of DMSO. Triethylamine (TEA) (2.00 ml, 14.30 mmol) was added and the solution stirred at room temperature for 24 h before quenching with 2N HCl (28.3 mmol). The solution was then dialyzed for 24 h against 1 L of distilled water using a dialysis membrane (Spectra/Por, MWCO 1000) and the retentate lyophilized. The NTA-PEG3400-VS product was stored at −20 °C until use. Yield: 50.3%. ^{1}H NMR ($CDCl_3$): δ 3.11-2.91 (br, CH_2CH_2O), 2.45 (t, J=6.0 Hz, $NHCH_2$), 1.88-1.53 (br, $NHCH_2(CH_2)_3CHCOOH$).

NTA-PEG3400-Si(OMe)$_3$—Silanation of NTA-PEG3400-VS was performed by free radical addition of mercaptopropyltrimethoxysilane (MPTS) to the vinyl sulfone substituent as shown in Scheme 1.[34,35] NTA-PEG3400-VS and an eight-fold excess of freshly distilled MPTS were added to toluene in a round bottom flask, followed by the addition of a 0.4-fold excess of 2,2′-azobisisobutyronitrile (AIBN) relative to NTA-PEG3400-VS. The mixture was stirred for 24 h at 60 °C under a N_2 atmosphere before precipitation of the product with anhydrous Et_2O. The precipitate was filtered, washed with excess Et_2O, and dried under reduced pressure to give NTA-PEG3400-Si(OMe)$_3$ as a white powder in 53% yield. ^{1}H NMR ($CDCl_3$): δ 3.9-3.15 (br, CH_2CH_2O), 2.45 (t, J=6.0 Hz, $NHCH_2$), 1.68-1.14 (br, $NHCH_2(CH_2)_3CHCOOH$), and 0.6 (CH_2Si).

Surface preparation and characterization

Silicon wafers or cover glasses were immersed into fresh piranha solution for 1 h and rinsed by bath sonication in deionized water. Piranha solution was prepared by mixing pure sulphuric acid and hydrogen peroxide (30% solution) in a 7:3 volume ratio. *Piranha solutions are potentially explosive and highly corrosive! Handle with extreme caution!* The clean substrates were dried under N_2 gas and then immersed in toluene solutions of mPEG5000-Si(OMe)$_3$ or NTA-PEG3400-Si(OMe)$_3$ (10 mg PEG derivative/ml) for 16 h at 60 °C.[35] The NTA-PEG3400-VS-modified surfaces were prepared as follows: piranha cleaned surfaces were immersed in 1% MPTS in toluene for 4 h and washed with toluene. The dried MPTS-modified surface was then incubated in NTA-PEG-VS (10 mg/ml) in 0.01M phosphate buffered saline (PBS) for 16 h at room temperature.[36]

Ellipsometric angles Δ and Ψ were measured on the PEG-grafted surfaces with an Auto ELII automatic null ellipsometer (Rudolph Research Corporation, Flanders, NJ) at two incident angles, 70° and 60°, using two wavelengths, 633 and 405 nm. Typically, five measurements were taken and the values averaged. First, the complex refractive index of the silicon wafer, n-ik, and the thickness and refractive index of the native oxide layer were obtained by fitting the Δ-Ψ values from the bare substrate at both angles. Details of the algorithm can be found in Cuypers *et al.*[37] For silicon, the optimal values were 3.84-0.018i and 5.36-0.300i at 633 nm and 405 nm, respectively. For silicon oxide, the refractive indices used were 1.465 and 1.470, respectively, for an oxide layer thickness of 3.1 nm. A four-layer model was then used to determine the thickness, d_1, and refractive index, n_1, of the dry polymer layer from the measured values of Δ and Ψ. The surface density, Γ, was determined from d_1 and n_1 at each angle and each wavelength by using the equation

$$\Gamma = d_1 \left(\frac{M}{A_r}\right)\left(\frac{n_1^2 - 1}{n_1^2 + 2}\right), \quad (1)$$

where M is the molecular weight and A_r is the molar refractivity of the polymer. From d_1 and the density ρ (assumed to be 1 g/cm^3), the average distance, L, between the grafted PEG chains, was determined from the deGennes equation

$$L = \left(\frac{M}{\rho d_1 N_A}\right)^{1/2} \quad (2)$$

where N_A is Avogadro's number.

X-ray photoelectron spectroscopy (XPS) experiments utilized a Kratos Axis ULTRA XPS instrument. All XPS spectra were obtained at 10^{-9} torr with monochromatized Al *K*α radiation as the X-ray source. A hemispherical analyzer with a multichannel detector was used with a takeoff angle of 90°. For survey, the dwell time was 0.1 s and the pass energy was 160 eV. For high resolution spectra, a pass energy of 40 eV and a dwell time of 0.3 s were used for Ni 2p, O 1s, and C 1s, and 0.5 s for N 1s.

The surface wettability of the PEG-modified surfaces that had been dried in a dessicator overnight was determined under static conditions using a Kruss contact angle goniometer (Hamburg, Germany).

Expression of hexahistidine-tagged green fluorescent protein (his$_6$-GFP)

Ampicillin-resistant *E. coli* that had been transfected with a gene to express wild-type his$_6$-GFP under L-(+)-arabinose induction were grown in Luria Broth (25 g LB/l L deionized water) containing ampicillin (0.05 mg/mL) for 24 h at 37 °C. L-(+)-Arabinose (0.2 mg/mL) was added and the incubation continued for 24 h at 30 °C. After centrifugation, the cell pellet was lysed with BugBuster™ (Novagen, San Diego, CA) protein extraction reagent and the supernatant concentrated by ultrafiltration (MW cutoff = 10 kD). The concentrated protein solution was then purified using a Ni^{2+}-activated IMAC column (Amersham Biosciences, Piscataway, NJ) and eluted with imidazole. Imidazole was removed by three sequential centrifugal desalting steps using 10 kD cutoff Centricon filter units to assure complete removal of imidazole. The final concentration of his$_6$-GFP was determined by Bradford Assay using BSA standards (Bio-Rad, Hercules, CA) and the purity confirmed by SDS-PAGE electrophoresis.

Calibration curves for his$_6$-GFP and streptavidin

Stock solutions of his$_6$-GFP and SA-AF were diluted in 10 mM HEPES buffer containing 20% glycerol to produce concentrations of 100 μM-1 mM and 100 nM-1.8 μM, respectively.[c] The diluted protein solutions were spotted on epoxy-terminated hydrophobic glass slides (Arrayit, Sunnyvale, CA) using a manual microarrayer (V&P Scientific Co., SD, USA). The delivery volume of the manual microarrayer pin was 50 nL and the diameters of the deposited solutions were 300 μm. Fluorescence intensities at each GFP or SA-AF spot were measured using confocal laser scanning microscopy (CLSM, Bio-Rad MC 1024, Bio-Rad Laboratories, Hercules, CA). The fluorescence intensities of ten individual spots were measured using the same instrument settings and the values averaged for each protein concentration. Surface density determinations were based on the delivery of the calibrated volume to a spot of known

[c]Glycerol was added as a humectant to prevent protein aggregation and dehydration during transfer and measurement of the surfaces, which could have affected the photophysical properties of the microcontact-printed chromophores.

diameter, the fluorescence intensity observed within the spot area, and the concentration of the protein applied to the spot.

Adsorption of his_6-GFP and his_6-biotin/SA-AF on NTA-PEG-modified surfaces

Surfaces modified with NTA-PEG3400-$Si(OMe)_3$, NTA-PEG3400-VS, or mPEG5000-$Si(OMe)_3$ were activated by treating them with 50 mM $NiCl_2$ for 1 h. To prime the surfaces for SA-AF binding, the Ni^{2+}-chelated surfaces were immersed in his_6-biotin solutions at concentrations ranging from 0.2 to 10 mg/ml in 0.01 M phosphate buffered saline, pH 7.4 (PBS) for 1 h at room temperature. The samples were then washed with PBS and the his_6-biotin modified surface incubated in SA-AF solutions for 2 h at room temperature. A final wash with PBS/0.1% Tween 20 was used to remove unbound streptavidin molecules.

Solutions containing varying concentrations of his_6-GFP were prepared in HEPES buffer. Ni^{2+}-chelating NTA-PEG surfaces were incubated in his_6-GFP solutions for 2 h and then rinsed with HEPES buffer. The fluorescence intensities of the protein-immobilized surfaces were then measured using CLSM as described above. Tests for specific binding were performed by incubating the surfaces with 500 mM imidazole in HEPES buffer for 10 min, followed by a HEPES buffer wash to remove the Ni^{2+}:NTA-bound his_6-protein that was desorbed via Ni^{2+}-stripping by excess imidazole. The fluorescence intensity was measured before and after the surfaces were exposed to imidazole and the difference attributed to non-specific binding.

Lipid vesicle preparation and immobilization on NTA-PEG3400-$Si(OMe)_3$-modified surfaces

A $CHCl_3$ solution of EPC:DOPE:NBD-DPPE (64:35:1 mol%) was evaporated under a gentle N_2 flow and dried under a 100μ vacuum for 4 h. The dried lipid mixture was then hydrated in HEPES buffer, suspended by vigorous vortexing, and dispersed by probe sonication (3 cycles of 10 min duration at 60W). The sample was immersed in an ice bath during sonication to prevent overheating. The resulting solution of small unilamellar vesicles (SUV) was clarified by centrifugation for 5 min at 5000 rpm and diluted to the desired concentrations. The average diameter of the lipid vesicles measured by dynamic light scattering (DLS) ranged between 90–130 nm.

His_6-gA and wild type gA solutions were prepared at various concentrations using a stock solution of the peptides in methanol (0.5 μM). These solutions (100 μl) were introduced by slow addition to 1 mL of a 1 mM SUV solution with gentle stirring. Lipid vesicles containing his_6-gA or wild type gA were incubated for 1 h on Ni^{2+}:NTA-PEG-modified surfaces and the fluorescence intensity determined by CLSM as previously described. Similar experiments were performed using SUV with a constant protein:lipid ratio at concentrations ranging from 0.1 mM to 10 mM.

Results and Discussion

Surface preparation and characterization

Two NTA-PEG derivatives, NTA-PEG3400-$Si(OMe)_3$ and NTA-PEG3400-VS, were prepared by lysine-NTA substitution of *N*-hydroxysuccinimide-activated-PEG-VS. These materials were grafted onto glass using either 1) direct chemisorption in toluene at 60 °C (NTA-PEG3400-$Si(OMe)_3$ and mPEG5000-$Si(OMe)_3$) or 2) conjugation with thiol-terminated, MPTS-modified glass in aqueous solution at room temperature (NTA-PEG3400-VS). Since the surface modification schemes using NTA-PEG3400-$Si(OMe)_3$ and NTA-PEG3400-VS ultimately produce the same surface-grafted molecules, we used both approaches to determine which procedure would generate the most densely PEGylated surfaces for NTA-mediated his_6-protein adsorption.

The thicknesses (d_1), refractive indices (n_1), surface densities (Γ), and average distances (L) between grafted chains of the PEG-grafted surfaces were determined by ellipsometry and contact angle measurements (Table 1). Generally, the ellipsometry results obtained using two different measurement angles were the same within experimental error for surfaces that were probed at $\lambda = 633$ nm. At $\lambda = 405$ nm, the calculated thicknesses at both measurement angles were slightly lower than those determined at $\lambda = 633$ nm, but the calculated refractive indices were higher, resulting in slightly higher surface densities. For NTA-PEG3400-VS-grafted surfaces, only the data at 70° are shown. Our experiments show that the thicknesses and surface densities of NTA-PEG3400-VS-grafted surfaces are considerably smaller than those of NTA-PEG3400-Si$(OMe)_3$- and mPEG5000-Si$(OMe)_3$-grafted surfaces, apparently due to lower grafting densities in the NTA-PEG3400-VS system. The thicknesses of the chemisorbed PEG layers were the same within experimental error at 70°, where the observed thicknesses were 14 ± 3 nm and 17 ± 3 nm for mPEG5000-Si$(OMe)_3$- and NTA-PEG3400-Si$(OMe)_3$-modified surfaces, respectively, while the NTA-PEG3400-VS-grafted surface thicknesses (4 ± 0 nm) were less than 25% of the chemisorbed PEG layer thickness. The differences in Γ and L for the three dried PEG layers had no effect on the water contact angles, which were 48° ± 2°, 51° ± 1°, and 51° ± 2° for mPEG5000-Si$(OMe)_3$, NTA-PEG3400-Si$(OMe)_3$ and NTA-PEG3400-VS, respectively. The contact angles were 30° for all the PEG-grafted surfaces upon storage for 1 d in contact with the normal laboratory atmosphere. All protein absorption experiments used surfaces immediately after the surface modification reactions were complete.

To gain insight into the structure of the grafted PEG layer, we compared the Flory diameter ($2R_f$) and the average distance (L) between PEG grafting sites among the different surface types.[38] The Flory radius, R_F, of PEG was estimated for a polymer comprised of N units, each of size a, from the following equation:

$$R_F = aN^{3/5}. \quad (3)$$

The average distance between the PEG chains calculated from the ellipsometric thicknesses at 70° were 6 Å for NTA-PEG3400-Si$(OMe)_3$, 8 Å for m-PEG5000-Si$(OMe)_3$, and 12 Å for NTA-PEG3400-VS (Table 1). The Flory diameters are 4.0 nm for PEG3400 and 5.1 nm for PEG5000 at a unit length of 3 Å.[39] Comparison between the average PEG grafting distances and the Flory diameters suggests that the PEG molecules are in the brush regime for the chemisorbed PEG derivatives as has been described for many other PEG-grafted surfaces.[13,24,40] The PEG molecules on the NTA-PEG3400-VS-grafted surfaces are less dense than the surfaces produced by direct trimethoxysilane-mediated chemisorption and are likely in the mushroom configuration, a finding that is consistent with other studies employing thiol-vinyl sulfone reactions for grafting PEG onto glass.[36,41] Since the PEG grafting density depends on temperature, solvent, and synthesis pathway,[41–43] the conditions chosen for the NTA-PEG3400-Si$(OMe)_3$ and mPEG5000-Si$(OMe)_3$ grafting reactions (60 °C in toluene) were below the PEG critical solution temperature. The repulsive forces of the PEG chains, which are lower at higher temperatures, leads to greater chain packing densities at the surface due to a smaller excluded volume.[43,44] The observed PEG layer density is also dependent on the concentration of pinning sites available at the surface.[43] The surface density of pinning sites is likely lower for the NTA-PEG3400-VS derivative than for the NTA-PEG3400-Si$(OMe)_3$ and mPEG5000-Si$(OMe)_3$ precursors because (1) the MPTS activation step required for NTA-PEG3400-VS grafting consumes two surface silanol groups for each MPTS molecule deposited and (2) some of the chemisorbed MPTS may become inactivated due to air oxidation during rinsing and handling.

NTA-PEG3400-Si$(OMe)_3$-modified surfaces were scanned using high resolution XPS analysis of C 1s and O 1s binding energies (Figure 1). Contributions from the ether carbon component at 286.5 eV, the C-H bond at 285 eV, and the COOH groups at 288 eV were observed in the C1s peaks of NTA-PEG3400-Si$(OMe)_3$-modified surfaces. A large contribution from the ether

carbon component in the C1s peak was observed relative to the peak of the bare silicone oxide surface, thus providing clear evidence of PEG on these surfaces.[38,45] Surfaces modified with NTA-PEG3400-Si(OMe)$_3$ and mPEG5000-Si(OMe)$_3$ were then treated with a Ni^{2+} solution and dried prior to XPS analysis. We were unable to detect a Ni signal from these samples at the expected energy of 856 eV, even though the presence of Ni^{2+} has been observed on NTA-functionalized self-assembled monolayers.[46,47] Since the surface density of NTA ligands is much lower on our PEG grafted surfaces than the previously reported NTA side chain polymers[46] and NTA self-assembled monolayers[47], we infer that the Ni^{2+} concentrations on these surfaces is too low to be detected.

His_6-GFP and his_6-biotin/streptavidin immobilization

Three model systems were used in this study to evaluate the immobilization properties of freshly prepared Ni^{2+}:NTA-PEG surfaces toward his_6-tag substrates—direct adsorption of his_6-GFP, sequential adsorption of his_6-biotin/SA-AF, and adsorption of his_6-gA, a hydrophobic peptide that was imbedded within fluid phase lipid vesicles (Figure 2). The surface densities of his_6-GFP and his_6-biotin/SA-AF immobilized on Ni^{2+}:NTA-PEG surfaces were monitored using fluorescence microscopy. Glycerol-containing solutions of his_6-GFP and SA-AF were prepared over a 1 nM-1.25 μM concentration range, spotted onto epoxy-coated glass cover slips and the calibration curve of normalized fluorescence intensity versus surface density of GFP and SA-AF determined (Supplementary Information). The resulting CLSM fluorescence images showed homogeneous distributions of both fluorescent proteins, with no evidence of crystallization or precipitation on the timescale of the measurements. The fluorescence intensities within ten spotted zones of equivalent area and concentration were then averaged using identical CLSM imaging conditions and converted to surface densities using the known amounts of his_6-GFP and SA-AF transferred by microcontact printing. The normalized fluorescence intensities thus obtained were linearly dependent on the surface densities of both proteins, enabling the use of these calibration curves for the determination of his_6-GFP and SA-AF surface concentrations under his_6-protein capture conditions.

To evaluate the ability of the different PEG-grafted surfaces toward SA-AF capture, NTA-PEG3400-Si(OMe)$_3$, NTA-PEG3400-VS, and mPEG5000Si(OMe)$_3$ modified surfaces were sequentially immersed in 50 mM Ni^{2+}, his_6-biotin (0.05–10μM), and 1 μg/ml SA-AF. The surface density of immobilized streptavidin increased as the concentration of his_6-biotin solution increased up to 1 μM (Figure 3A). A second set of PEG-modified surfaces were sequentially immersed in solutions of 50 mM Ni^{2+}, 1 μM his_6-biotin, and SA-AF solutions of increasing concentration to probe the effects of streptavidin surface loading at constant biotin concentration (Figure 3B). The maximum streptavidin surface density achieved was 90 fmol/cm^2 on surfaces that were modified with NTA-PEG3400-Si(OMe)$_3$.

His_6-GFP adsorption on PEG-grafted surfaces was also determined using the same approach (Figure 4). As observed for the his_6-biotin/SA-AF system, we found that the his_6-GFP surface densities increased on NTA-PEG-grafted surfaces as the his_6-GFP solution concentration increased. The maximum his_6-GFP surface density achieved was 45 pmol/cm^2 on surfaces that were modified with NTA-PEG3400-Si(OMe)$_3$.

NTA-PEG3400-Si(OMe)$_3$ surfaces displayed the highest surface densities of immobilized his_6-biotin/SA-AF and his_6-GFP compared to surfaces modified with either NTA-PEG3400-VS or mPEG5000-Si(OMe)$_3$ (Figures 3B and 4). Given the well-known capability of mPEG-coated surfaces to minimize protein adsorption[48], it was expected that the surface densities of his_6-GFP and his_6-biotin/SA-AF would be low on mPEG5000-Si(OMe)$_3$-modified surfaces that lack the Ni^{2+}:NTA affinity ligand. Indeed, the binding of his_6-GFP and his_6-biotin/SA-AF on NTA-PEG surfaces is the result of a competition between PEG repulsion of the protein adsorbate and Ni^{2+}:NTA attraction of the protein via the his_6 affinity ligand. Grafted polymer

chains are known to adopt conformations in which steric hindrance between neighboring polymer chains and apposed surfaces, such as bound proteins and lipid vesicles, is avoided. Szleifer and coworkers have determined the minimum free energy of grafted polymers over a wide range of grafting densities.[49,50] They have also described the attractive forces of polymer end groups which determine the maximum adsorption possible via specific interactions when the grafting density has been optimized.[50] Our results support the predictions that protein adsorption is highly dependent on the magnitude of the attractive forces of the end groups and the grafting density of PEG. These findings underscore the importance of optimizing both the strength and surface density of affinity ligands, as well as the underlying structure of the grafted polymer layer, to provide precise control over a bound protein layer via specific interactions.

Since we were unable to directly detect the presence of nickel ions on Ni^{2+}:NTA-PEG3400-modified surfaces, we performed a ligand competition experiment to indirectly establish the presence of this chelated metal ion. Reversible binding of his_6-proteins to the Ni^{2+}:NTA-modified surface was probed by addition of a large excess of imidazole, which removes Ni^{2+} from the his_6-protein:Ni^{2+}:NTA complex via ligand competition. As the data in Figure 5 show, his_6-GFP immobilized on the NTA-PEG3400-$Si(OMe)_3$-grafted surface was fully displaced by the addition of 500 mM imidazole. We infer from the significant reduction in GFP fluorescence intensity after imidazole addition that the NTA-PEG3400-$Si(OMe)_3$-grafted surface contained ligated Ni^{2+} ions that were responsible for specific binding of his_6-GFP.

Lipid vesicle immobilization via his_6-gA

gA, a pentadecapeptide composed of alternating D- and L-amino acids, forms a β helix that spans one monolayer of bilayer membranes. When two gA helices present in opposing monolayer leaflets hydrogen bond via their N-termini, they can dissipate ion gradients across the membrane by transporting positive monovalent ions through the dimeric channel. This property of gA has been exploited as the responsive element of an ion-sensitive supported membrane biosensor.[9,51] In this study, gA was modified with a hexahistidine affinity tag at its C terminus,[9] since it is known that this modification does not interfere with the activity of gA.[9,52] Wild type gA and his_6-gA were then inserted into preformed lipid vesicles by slow addition of methanolic solutions of the peptides to the vesicle solutions with stirring. Since his_6-gA was assumed to be incapable of flip-flop into the inner layer of the lipid bilayer from the outer membrane monolayer because transport of the hydrophilic hexahistidine sequence through the hydrophobic core of the lipid bilayer would be required, we expected that his_6-gA is only associated with the outer leaflet of the bilayer lipid vesicles.

His_6-gA-containing lipid vesicle adsorption was then examined using Ni^{2+}:NTA-PEG3400-$Si(OMe)_3$-grafted surfaces. Changes in adsorption as a function of the gA:lipid ratio, R, was probed by measuring the fluorescence intensity of Ni^{2+}:NTA-bearing coverslips that were exposed to lipid vesicles comprised of 1 mM EPC:DOPE:NBD-DPPE (64:35:1) in HEPES buffer. Fluorescence intensity from the surface increased as the his_6-gA composition in the membrane increased due to his_6-gA:Ni^{2+}:NTA-mediated vesicle adsorption. Control experiments using gA-free and wild type gA vesicles produced very little fluorescence from the Ni^{2+}:NTA-PEG3400-$Si(OMe)_3$-grafted surfaces, indicating that nonspecific adsorption of lipid vesicles onto these surfaces is not significant. Specific vesicle adsorption was optimized using lipid vesicles containing 1:375 his_6-gA:lipid (Figure 6A). Exposure of various lipid concentrations ranging from 0.01–10 mM total lipid at 1:375 his_6-gA:lipid ratios was also examined to establish the maximum surface loading of vesicles at this composition. Our results show that his_6-gA lipid vesicle adsorption increases with increasing vesicle concentration (Figure 6B), with surface saturation occurring at 0.5 mM lipid.

In summary, we evaluated the protein capture efficiencies of the NTA-PEG-grafted surfaces were evaluated by measuring fluorescence intensities PEGylated surfaces after exposure to

his_6-tag species. Protein immobilization was most effective for NTA-PEG3400-$Si(OMe)_3$-modified surfaces when direct his_6-protein:Ni^{2+}:NTA ligation was used; the areal densities achieved when multiple adsorption steps were required (e.g., his_6-biotin/SA-AF) led to greatly reduced levels of adsorbed protein. Lipid vesicles containing his_6-gA in a 1:375 gA:lipid ratio could also be immobilized on Ni^{2+}:NTA-PEG3400-$Si(OMe)_3$-modified surfaces. These experiments show that specific and reversible binding to PEG-modified silica surfaces occurred only when the PEG molecule contained a Ni^{2+}-activated NTA ligand and the protein possessed a hexahistidine interaction with the Ni^{2+}:NTA-PEG-grafted surface.

Conclusions

A novel NTA-PEG derivative that is capable of efficiently immobilizing his_6-proteins on silica surfaces has been synthesized using two different reaction pathways. XPS, contact angle, ellipsometry, and fluorescence confocal laser scanning microscopy characterization shows that areal densities up to 45 pmol/cm^2 his_6-GFP and 95 fmol/cm^2 his_6-biotin/SA-AF can be immobilized on silica that has been modified using a simple NTA-PEG3400-$Si(OMe)_3$ chemisorption procedure. Reversible binding was observed on Ni^{2+}:NTA-PEG3400-Si $(OMe)_3$-modified surfaces for his_6-GFP and his_6-biotin/SA-AF. Taken together, our results show that NTA-PEG conjugates appear to provide an ideal blend of characteristics for promoting specific adsorption of his_6-proteins or vesicles containing his_6-tag species via the distal NTA moiety without compromising the intrinsic property of PEG to reduce non-specific adsorption of proteins or vesicles onto the underlying substrate. Our results also suggest that NTA-PEG-modified surfaces may provide a general and powerful method for immobilizing soluble and integral membrane proteins with control over 1) orientation relative to the solid support, 2) areal density and 3) spacing between the immobilized protein and the solid substrate. Control over these features is essential for the practical realization of membrane protein-based biosensors. Further development of these NTA-PEG molecules and grafting techniques are in progress for monitoring the activity of Ste14p,[53] a isoprenylcysteine carboxyl methyltransferase involved in Ras signal transduction.

Supplementary Material

Refer to Web version on PubMed Central for supplementary material.

Acknowledgements

This research was supported by NIH CA112427 and the Indiana 21st Century Fund. The authors would like to thank Kyung-Jae Jeong for his help with the XPS measurements and Richard T. Haasch (Center for Microanalysis at the University of Illinois, Champaign-Urbana) for his technical assistance with the XPS. The XPS facility is partially supported by the U.S. Department of Energy under grant DEFG02-91-ER45439.

References

1. Sackmann E. Supported membranes: scientific and practical applications. Science 1996;271:43. [PubMed: 8539599]
2. Bieri C, Ernst OP, Heyse S, Hofmann KP, Vogel H. Micropatterneed immobilization of a G-protein-coupled receptor and direct detection of G protein activation. Nature Biotech 1999;17:1105.
3. Stora T, Lakey JH, Vogel H. Ion-channel gating in transmembrane receptor proteins: functional activity in tethered lipid membranes. Angew Chem Int Ed 1999;38:389.
4. Terrettaz S, Ulrich WP, Guerrini R, Verdini A, Vogel H. Immunosensing by a synthetic ligand-gated ion channel. Angew Chem Int Ed 2001;40:1740.
5. Ataka K, Giess F, Knoll W, Naumann R, Haber-Pohlmeier S, Richter B, Heberle J. Oriented attachment and membrane reconstitution of his-tagged cytochrome *c* oxidase to a gold electrode: in situ monitoring

by surface-enhanced infrared absorption spectroscopy. J Am Chem Soc 2004;126:16199. [PubMed: 15584756]

6. Sevin-Landais A, Rigler P, Tzartos S, Hucho F, Hovius R, Vogel H. Functional immobilization of the nicotinic acetylcholine receptor in tethered lipid membranes. Biophys Chem 2000;85:141. [PubMed: 10961502]
7. Krishna G, Schulte J, Cornell BA, Pace R, Osman PD. Tethered bilayer membranes containing ionic reservoirs: Selectivity and conductance. Langmuir 2003;19:2294.
8. Larsson C, Bramfeldt H, Wingren C, Borrebaeck C, Höök F. Gravimetric antigen detection utilizing antibody-modified lipid bilayers. Anal Biochem 2005;345:72. [PubMed: 16139234]
9. Stora T, Dienes Z, Vogel H, Duschl C. Histidine-tagged amphiphiles for the reversible formation of lipid bilayer aggregates on chelator-functionalized gold surface. Langmuir 2000;16:5471.
10. Lahiri J, Kalal P, Frutos AG, Jonas SJ, Schaeffler R. Method for fabricating supported bilayer lipid membranes on gold. Langmuir 2000;16:7805.
11. Elliott JT, Burden DL, Woodward JT, Sehgal A, Douglas JF. Phospholipid monolayers supported on spun cast polystyrene films. Langmuir 2003;19:2275.
12. Seitz M, Ter-Ovanesyan E, Hausch M, Park CK, Zasadzinski JA. Formation of tethered supported bilayers by vesicle fusion onto lipopolymer monolayers promoted by osmotic stress. Langmuir 2000;16:6067.
13. Wagner ML, Tamm LK. Tethered polymer-supported planar lipid bilayers for reconstitution of intergral membrane proteins: silane-polyethyleneglycol-lipid as a cushion and covalent linker. Biophys J 2000;79:1400. [PubMed: 10969002]
14. Naumann CA, Prucker O, Lehmann T, Ruhe J, Knoll W, Frank CW. The polymer-supported phospholipid bilayer: tethering as a new approach to substrate-membrane stabilization. Biomacromolecules 2002;3:27. [PubMed: 11866552]
15. Theato P, Zentel R. Formation of lipid bilayers on a new amphiphilic polymer support. Langmuir 2000;16:1801.
16. Shen WW, Boxer SG, Knoll W, Frank CW. Polymer-supported lipid bilayers on benzophenone-modified substrates. Biomacromolecules 2001;2:70. [PubMed: 11749157]
17. Baumgart T, Offenhausser A. Polysaccharide-supported planar bilayer lipid model membranes. Langmuir 2003;19:1730.
18. Wagner ML, Tamm LK. Reconstituted syntaxin1A/SNAP25 interacts with negatively charged lipids as measured by lateral diffusion in planar supported bilayers. Biophys J 2001;81:266. [PubMed: 11423412]
19. Munro JC, Frank CW. In situ formation and characterization of poly(ethylene glycol)-supported lipid bilayers on gold surfaces. Langmuir 2004;20:10567. [PubMed: 15544386]
20. Tanaka M, Sackmann E. Polymer-supported membranes as models of the cell surface. Nature 2005;437:656. [PubMed: 16193040]
21. Schmid EL, Keller TA, Dienes Z, Vogel H. Reversible oriented surface immobilization of functional proteins on oxide surfaces. Anal Chem 1997;69:1979. [PubMed: 9183172]
22. Rigler P, Ulrich WP, Hoffman P, Mayer M, Vogel H. Reversible immobilization of peptides: Surface modification and in situ detection by attenuated total reflection FTIR spectroscopy. Chem Phys Chem 2003;4:268. [PubMed: 12674599]
23. Jacobsen K, Oga S, Hubbell WL, Risse T. Determination of the orientation of T4 lysozyme vectorially bound to a planar-supported bilayer using site-directed spin labeling. Biophys J 2005;88:4351. [PubMed: 15778448]
24. Lata S, Piehler J. Stable and functional immobilization of histidine-tagged proteins via multivalent chelator headgroups on a molecular poly(ethylene glycol) brush. Anal Chem B 2005;77:1096.
25. Sigal GB, Bamdad C, Barberis A, Strominger J, Whitesides GM. A self-assembled monolayer for the binding and study of histidine-tagged proteins by surface plasmon resonance. Anal Chem 1996;68:490. [PubMed: 8712358]
26. Kroger D, Hucho F, Vogel H. Ligand binding to nicotinic acetylcholine receptor investigated by surface plasmon resonance. Anal Chem 1999;71:3157.

27. Wegner GJ, Lee HJ, Marriott G, Corn RM. Fabrication of histidine-tagged fusion protein arrays for surface plasmon resonance imaging studies of protein-protein and protein-DNA interactions. Anal Chem 2003;75:4740. [PubMed: 14674449]
28. Gamsjaeger R, Wimmer B, Kahr H, Tinazli A, Picuric S, Lata S, Tampé R, Maulet Y, Gruber HJ, Hinterdorfer P, Romanin C. Oriented binding of his_6-tagged carboxyl-tail of the L-type Ca^{2+} channel a_1-subunit to a new NTA-functionalized self-assembled monolayer. Langmuir 2004;20:5885. [PubMed: 16459605]
29. Lee JK, Kim YG, Chi YS, Yun WS, Choi IS. Grafting nitrilotriacetic groups onto carboxylic acid-terminated self-assembled monolayers on gold surfaces for immobilization of histidine-tagged proteins. J Phys Chem B 2004;108:7665.
30. Tinazli A, Tang J, Valiokas R, Picuric S, Lata S, Piehler J, Liedberg B, Tampé R. High-affinity chelator thiols for switchable and oriented immobilization of histidine-tagged proteins: a generic platform for protein chip technologies. Chem Eur J 2005;11:5249.
31. Dawson RJP, Locher KP. Structure of a bacterial multidrug ABC transporter. Nature 2006;443:180. [PubMed: 16943773]
32. Schmitt L, Dietrich C, Tampé R. Synthesis and characterization of chelator-lipids for reversible immobilization of engineered proteins at self-assembled lipid interfaces. J Am Chem Soc 1994;116:8485.
33. Zhou M, Haldar S, Franses J, Kim JM, Thompson DH. Synthesis and self-assembly properties of acylated cyclodextrins and nitrilotriacetic acid (NTA)-modified inclusion ligands for interfacial protein crystallization. Supramol Chem 2005;17:101.
34. Pale-Grosdemange C, Simon ES, Prime KL, Whitesides GM. Formation of self-assembled monolayers by chemisorption of derivatives of oligo(ethylene gycol) of structure $HS(CH_2)_{11}(OCH_2CH_2)_mOH$ on gold. J Am Chem Soc 1991;113:12.
35. Jo S, Park K. Surface modification using silanated poly(ethylene glycol)s. Biomaterials 2000;21:605. [PubMed: 10701461]
36. Perret E, Leung A, Morel A, Feracci H, Nassoy P. Versatile decoration of glass surfaces to probe individual protein-protein interaction and cellular adhesion. Langmuir 2002;18:846.
37. Cuypers PA, Corsel JW, Janssen MP, Kop JMM, Hermens WT, Hemker HC. The adsorption of prothrombin to phosphatidylserine multilayers quantitated by ellipsometry. J Biol Chem 1983;258:2426. [PubMed: 6822569]
38. Sofia SJ, Premnath V, Merrill EW. Poly(ethylene oxide) grafted to silicon surfaces: Grafting density and protein adsorption. Macromolecules 1998;31:5059. [PubMed: 9680446]
39. Yang Z, Galloway JA, Yu H. Protein interactions with poly(ethylene glycol) self assembled monolayers on glass substrates: Diffusion and adsorption. Langmuir 1999;15:8405.
40. Otsuka H, Nagasaki Y, Kataoka K. Self-assembly of poly(ethylene glycol)-based block copolymers for biomedical applications. Curr Op Coll Interfac Sci 2001;6:3.
41. Nivens DA, Conrad DW. Photoactive poly(ethylene glycol) organosilane films for site specific protein immobilization. Langmuir 2002;18:499.
42. McGovern ME, Kallury KMR, Thompson M. Role of solvent on the silanization of glass with octadecyltrichlorosilane. Langmuir 1994;10:3607.
43. Kingshott P, Thissen H, Giesser HJ. Effect of cloud-point grafting, chain length, and density of PEG layers on competitive adsorption of ocular proteins. Biomaterials 2002;23:2043. [PubMed: 11996046]
44. Emoto K, Harris JM, Alstine JM. Grafting poly(ethylene glycol) epoxide to amino-derivatized quartz: Effect of temperature and pH on grafting density. Anal Chem 1996;68:3751.
45. Roure OD, Debiemme-Chouvy C, Malthete J, Silberzan P. Functionalizing surfaces with nickel ions for the grafting of protein. Langmuir 2003;19:4138.
46. Tang AJ, Wang C, Stewart R, Kopecek J. Self-assembled peptides exposing epitopes recognizable by human lymphoma cells. Bioconj Chem 2000;11:363.
47. Luk YY, Tingey ML, Hall DJ, Israel BA, Murphy CJ, Bertics PJ, Abbott NA. Using liquid crystals to amplify protein-receptor interactions: design of surfaces with nanometer-scale topography that present histidine-tagged protein receptors. Langmuir 2003;19:1671.

48. Mcpherson T, Kidane A, Szleifer I, Park K. Prevention of protein adsorption by tethered poly(ethylene oxide) layers: experiments and single-chain mean-field analysis. Langmuir 1998;14:176.

49. Szleifer I. Protein adsorption on tethered polymer layers. Effect of polymer chain architecture and composition. Physica A 1997;244:370.

50. Carignano MA, Szleifer I. Adsorption of model charged proteins on charged surfaces with grafted polymers. Mol Phys 2002;100:2993.

51. Kim JM, Patwardhan A, Bott A, Thompson DH. Preparation and electrochemical behavior of gramicidin bipolar lipid monolayer membranes supported on gold electrodes. Biochim Biophys Acta 2003;1617:10. [PubMed: 14637015]

52. Lougheed T, Borisenko V, Hand CE, Woolley GA. Fluorescent gramicidin derivatives for single-molecule fluorescence and ion channel measurements. Bioconj Chem 2001;12:594.

53. Febo-Ayala W, Morera-Felix S, Hrycyna CA, Thompson DH. Functional reconstitution of the integral membrane enzyme, isoprenylcysteine carboxyl methyltransferase, in synthetic bolalipid membrane vesicles. Biochemistry 2006;45:14683. [PubMed: 17144661]

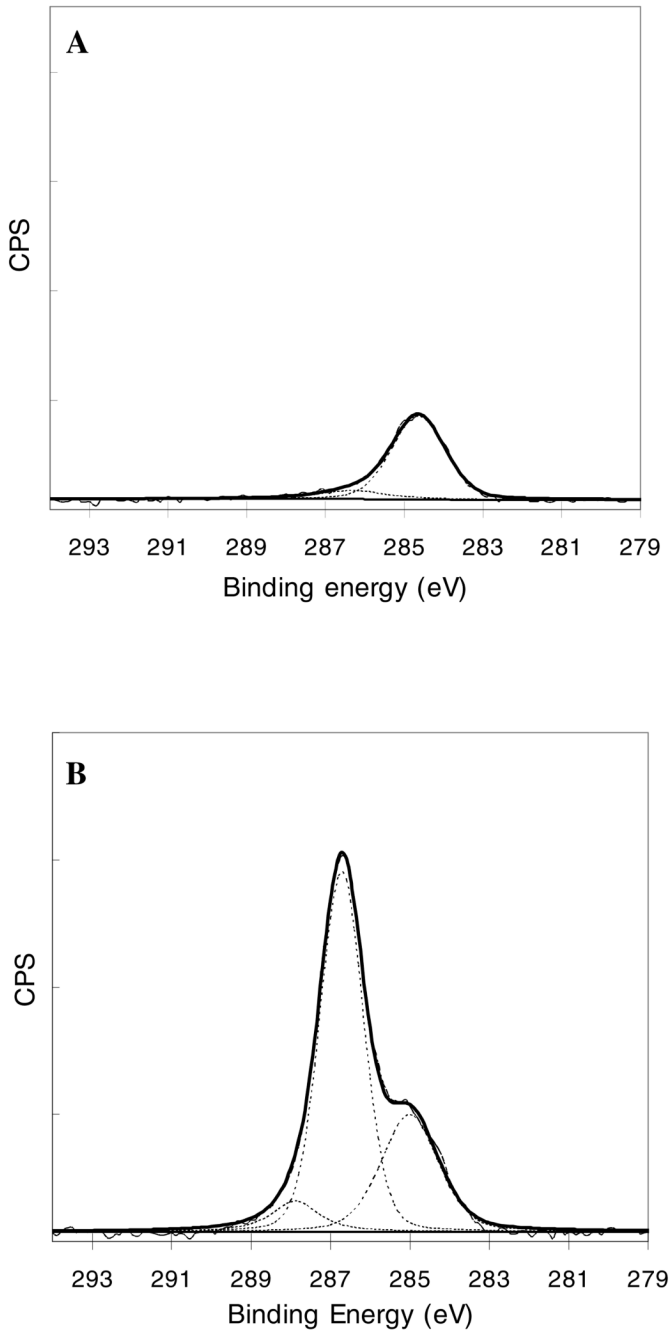

Figure 1.
C1s XPS spectra of (A) a bare silicone oxide surface and (B) a NTA-PEG3400-$Si(OMe)_3$-modified surface.

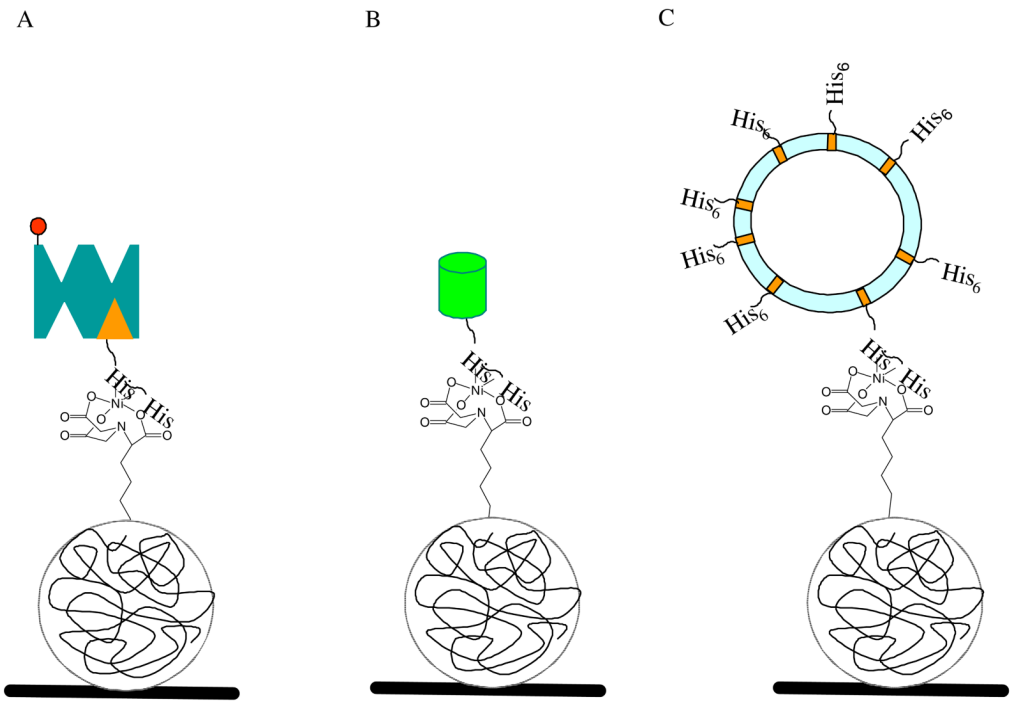

Figure 2.
Interaction between a PEG containing layer and a protein or a lipid vesicle: (A) Ni^{2+}:NTA-PEG-containing layer interacting with his_6-biotin and steptavidin-AlexaFluor555 (SA-AF); (B) Ni^{2+}:NTA-PEG-containing layer interacting with his_6-GFP; and (C) Ni^{2+}:NTA-PEG-containing layer interacting with a his_6-gA-containing lipid vesicle.

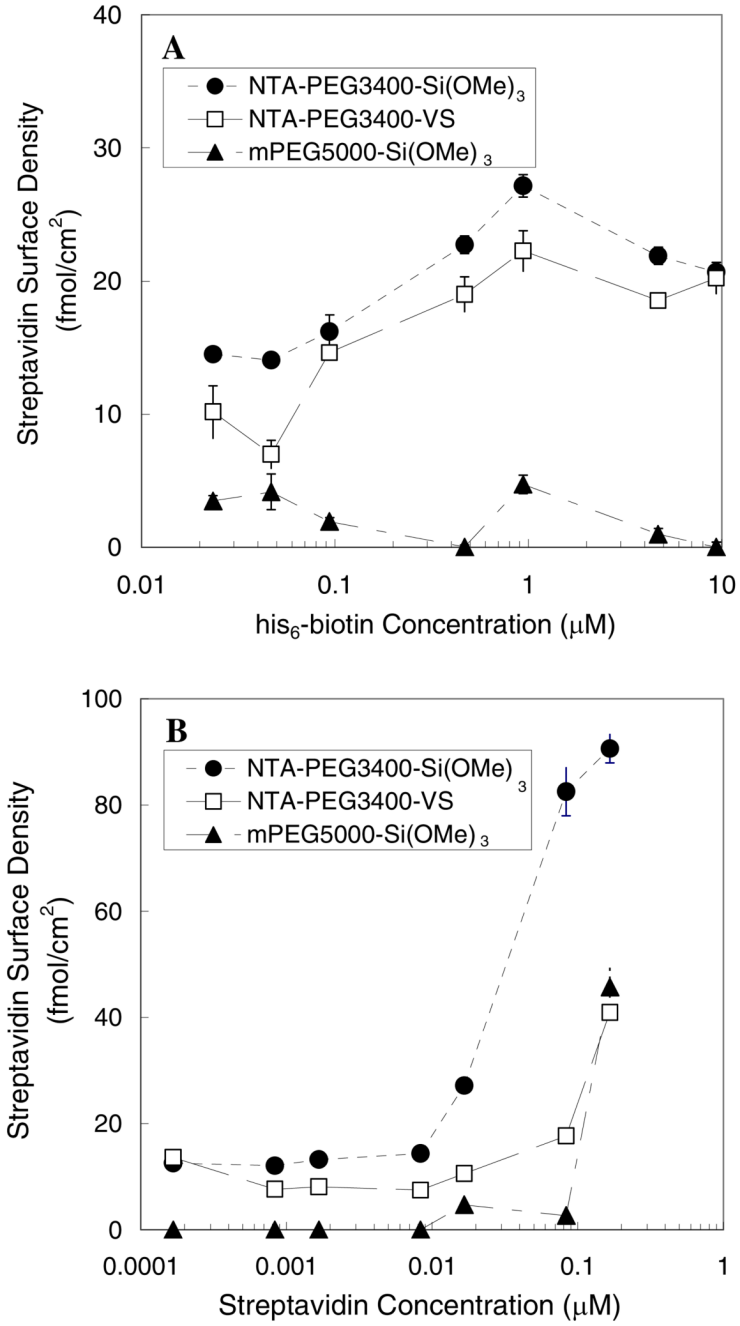

Figure 3.

The surface density of streptavidin as a function of (A) his_6-biotin concentration or (B) SA-AF concentration. PEG-modified surfaces were sequentially exposed to (A) 50 mM Ni^{2+} solution, different concentrations of his_6-biotin solution, and finally 1 μg/ml SA-AF solution or (B) 40 mM Ni_{2+} solution and 1 mg/ml his_6-biotin, followed by different concentrations of SA-AF solution. The lines serve as a guide to the eye.

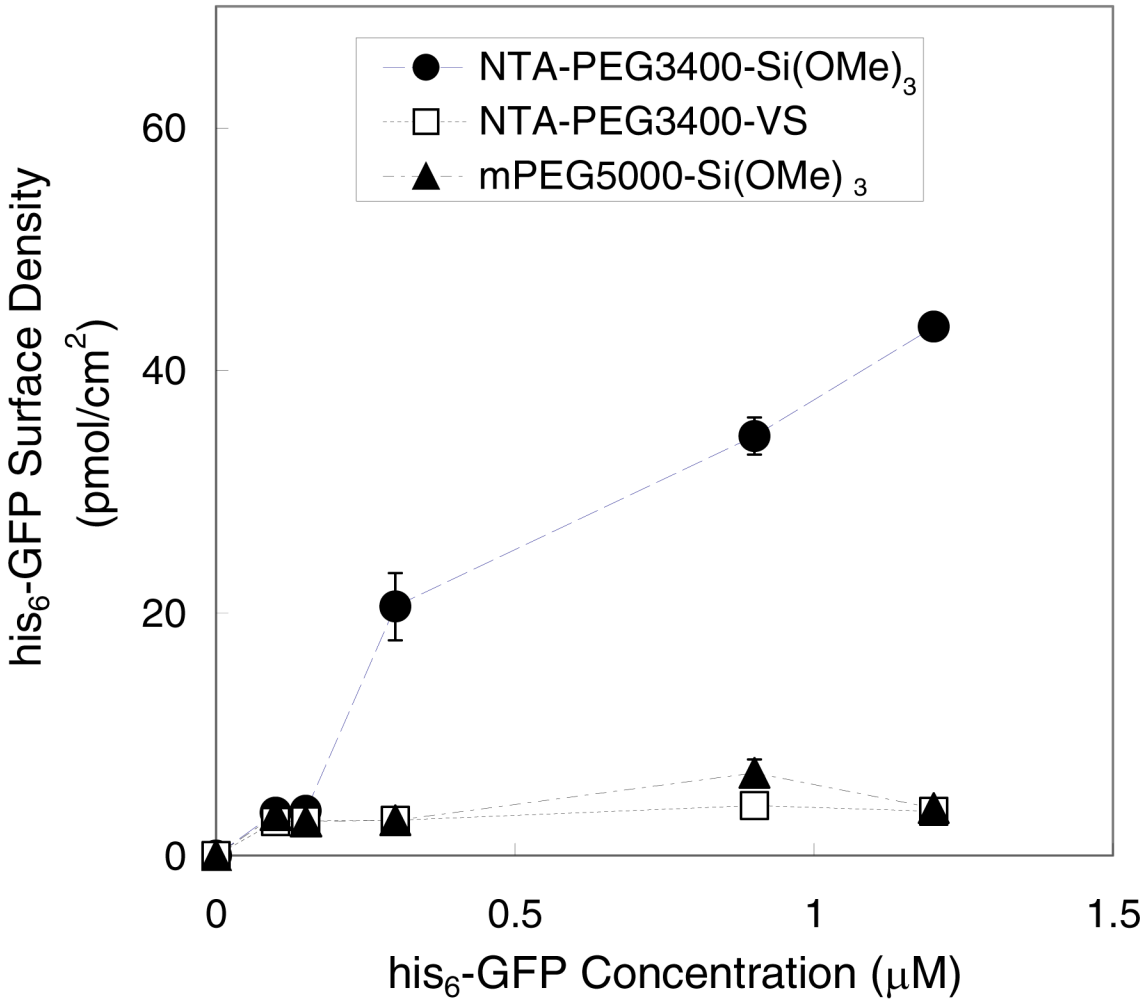

Figure 4.
Immobilization of his_6–GFP on PEG-modified surfaces, after activation with 50 mM Ni^{2+}, as a function of his_6-GFP concentration. The lines serve as a guide to the eye.

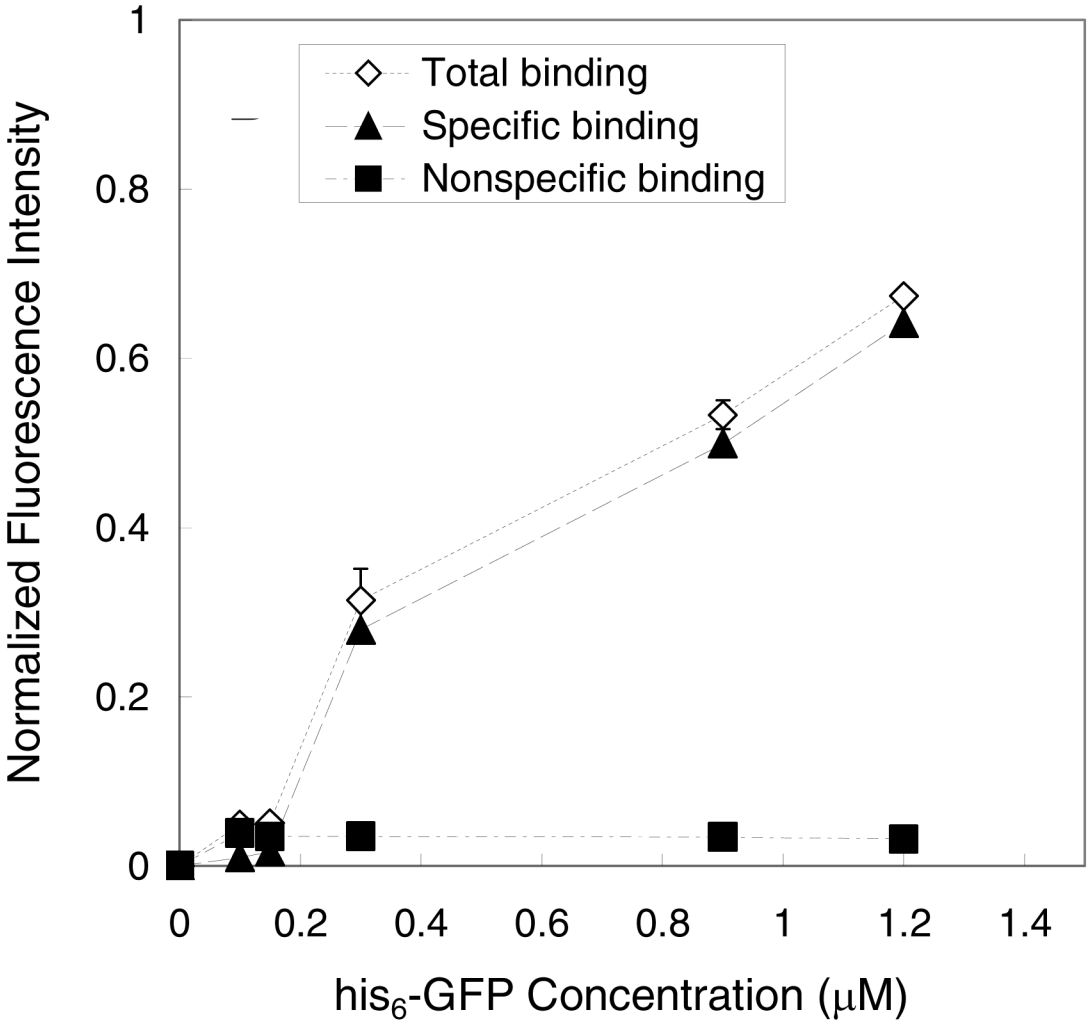

Figure 5.
Immobilization of his_6–GFP on NTA-PEG3400-$Si(OMe)_3$-modified surfaces, represented as normalized fluorescence intensity, as a function of his_6-GFP concentration. The total binding and nonspecific binding (i.e., after washing the his_6-GFP-loaded surface with 500 mM imidazole) on the NTA-PEG surface were measured. Specific binding was calculated as the difference between total binding and nonspecific binding.

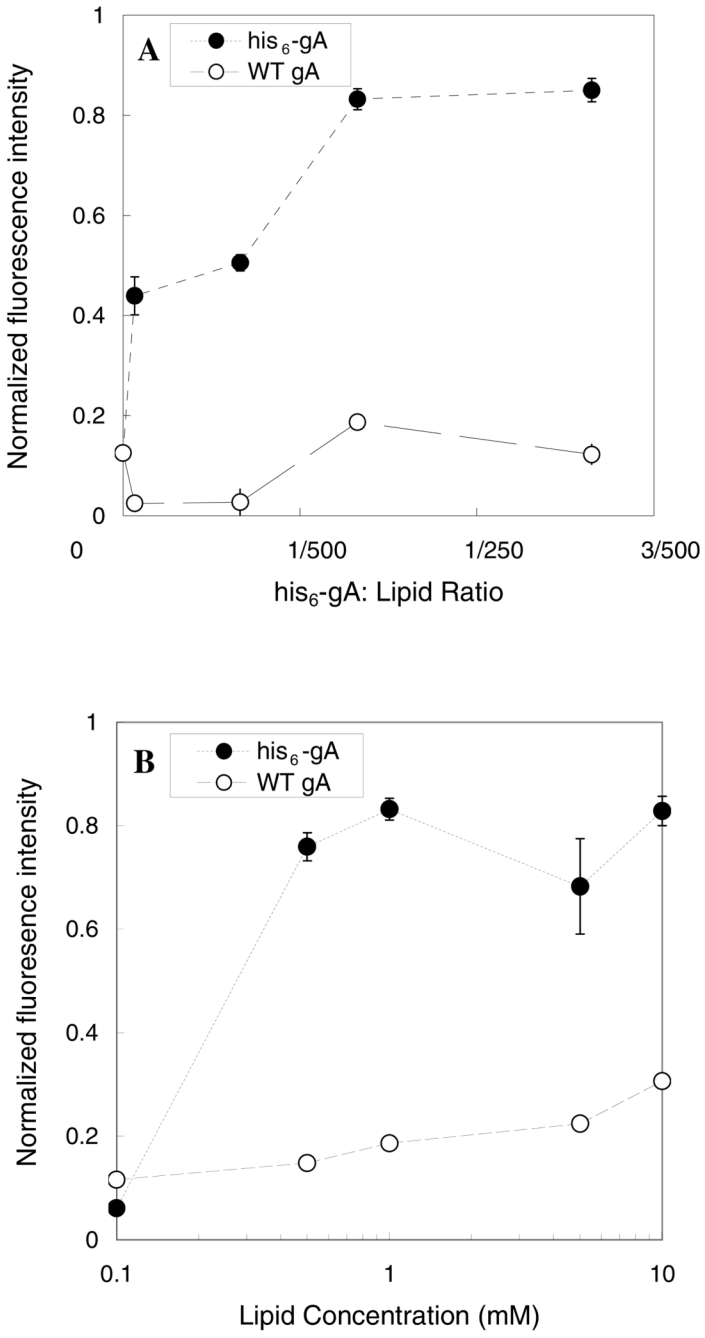

Figure 6.
The normalized fluorescence intensity as a function of (A) the gA:lipid ratio at 1 mM lipid vesicle concentration or (B) the lipid vesicle concentration at a constant gA:lipid ratio of 1:375.

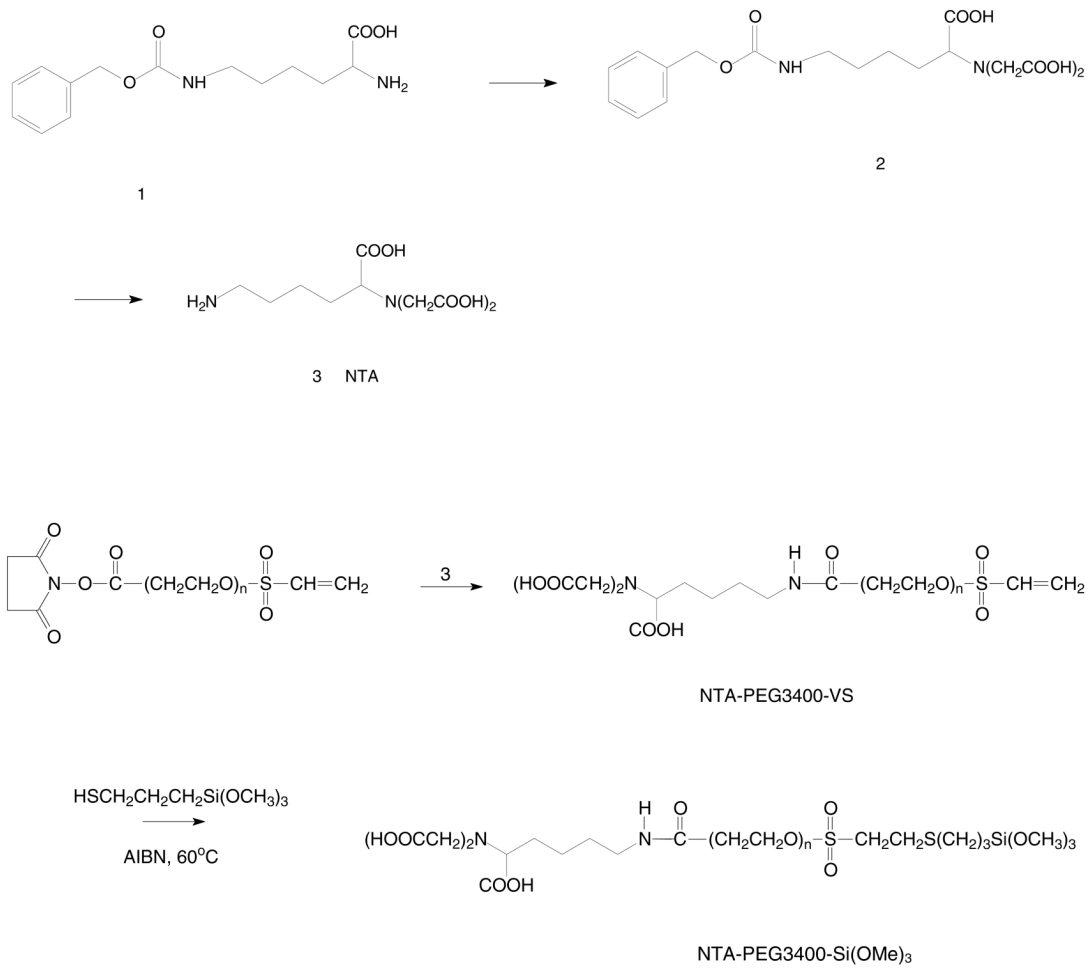

Scheme 1.
Synthesis scheme for NH_2-NTA, NTA-PEG3400-VS and NTA-PEG3400-Si$(OMe)_3$.

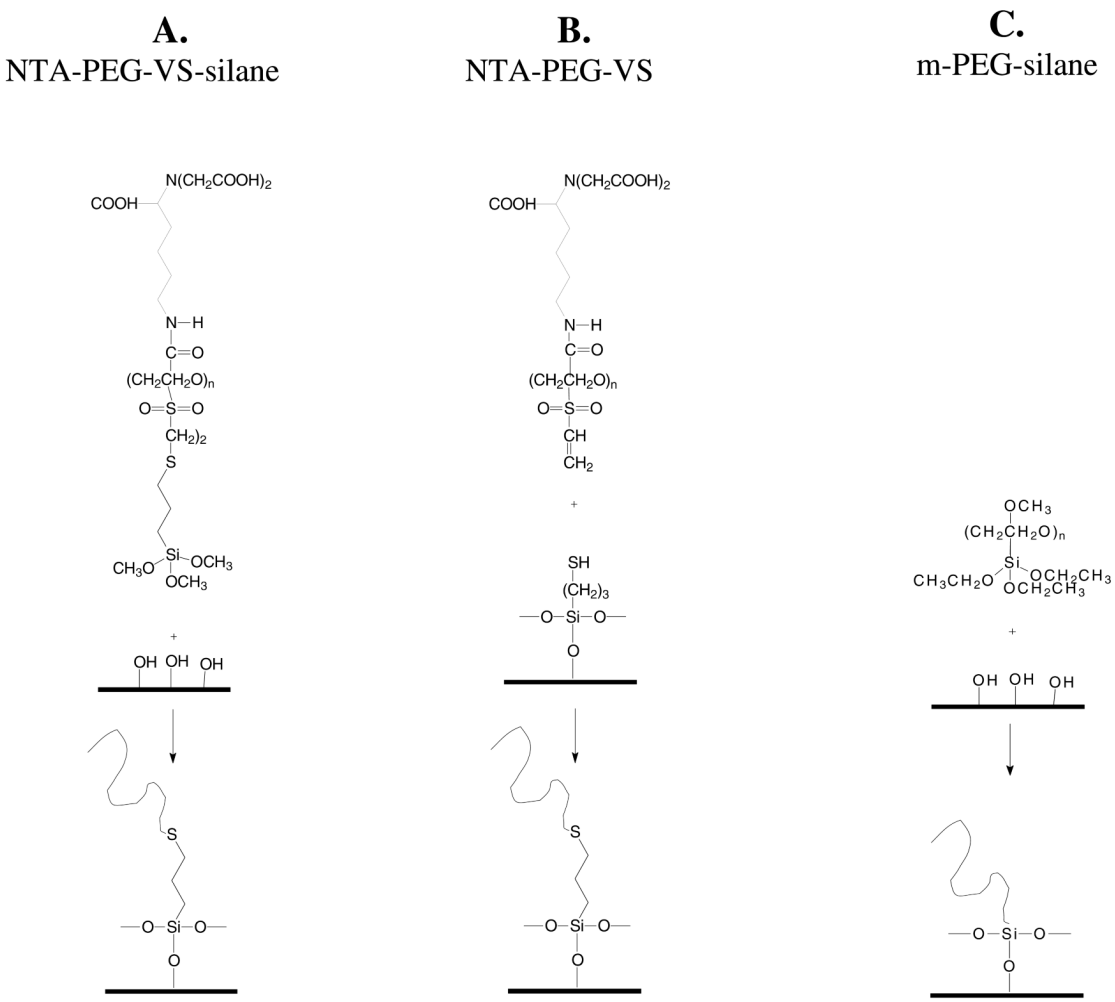

Scheme 2.
Methods for modifying silica with NTA-PEG3400-Si(OMe)$_3$, NTA-PEG3400-VS, and mPEG5000-Si(OMe)$_3$.

Table 1

Analysis of PEG modified surfaces by ellipsometry and contact angle measurements.

		mPEG5000-Si(OMe)$_3$		**NTA-PEG3400-Si(OMe)$_3$**		**NTA-PEG3400-VS + MPTS**
Φ (°)		70	60	70	60	70
633 nm	d_1 (nm)	14 ± 3	16 ± 1	17 ± 3	16 ± 1	4 ± 0
	n_1	1.436 ± 0.176	1.362 ± 0.057	1.346 ± 0.119	1.361 ± 0.064	1.703 ± 0.255
	Γ (μmol/m^2)	2.9 ± 0.2	2.8 ± 0.2	4.3 ± 0.2	4.2 ± 0.3	2.0 ± 0.3
	L (Å)	8 ± 1	7 ± 0	6 ± 1	6 ± 0	12± 0
405 nm	d_1 (nm)	13 ± 1	14 ± 0	13 ± 1	14 ± 1	3 ± 0
	n_1	1.529 ± 0.124	1.478 ± 0.042	1.545 ± 0.113	1.472 ± 0.074	1.747 ± 0.287
	Γ (μmol/m^2)	3.2 ± 0.3	3.2 ± 0.2	4.8 ± 0.4	4.6 ± 0.4	1.7 ± 0.1
	L (Å)	8 ± 1	8 ± 0	7 ± 0	6 ± 1	14 ± 0
Contact angle (°)		48° ± 2°		51° ± 1°		51° ± 2°